Journal of Information Systems Engineering and Management
2025, 10(17s)
e-ISSN: 2468-4376
https://www.jisem-journal.com/ **Research Article**

Advancing Brain Tumor Detection: A Comparative Study of Densenet and Resnet Architectures in MRI Analysis

[1]Para Rajesh, [2]A.Pramod Kumar, [3]Dr G Shyama Chandra Prasad, [4]Dr J Srinivas [5]Yuvaraju Macha

[1]Assistant Professor, Department of Computer Science and Engineering VNR Vignana Jyothi Institute of Engineering and Technology Hyderabad – 500090 Telangana, India.
rajesh_p@vnrvjiet.in
[2]Assistant Professor, Department of (CSE-CyS ,DS) and AI & DS VNR Vignana Jyothi Institute of Engineering and Technology Hyderabad – 500090 Telangana, India.
pramodkumar_a@vnrvjiet.in
[3]Professor, Department IT Matrusri Engineering College Hyderabad – 500059 Telangana, India.
gscprasad@gmail.com
[4]Associate Professor, Department IT Matrusri Engineering College Hyderabad – 500059 Telangana, India.
gscprasad@gmail.com
[5]Associate Professor, Department of Mathematics Matrusri Engineering College Hyderabad – 500059 Telangana, India.
yuvaraju.macha@matrusri.edu.in

ARTICLE INFO

Received: 05 Dec 2024
Revised: 24 Jan 2025
Accepted: 08 Feb 2025

ABSTRACT

In evaluating brain malignancies, radiologists frequently look at several MRI sequences produced by multimodal imaging. Advanced MRI techniques that seek to correlate histological characteristics with radiological markers like cellular density or vascular structure have recently been the focus of neuro-oncology research. Currently, the most used imaging methods in clinical practice are T1-weighted sequences, which highlight anatomical characteristics, and T2-weighted sequences, which display oedema and can assist in determining cellularity. It is still challenging for radiologists to diagnose suspected gliomas or brain lesions on MRI using histological subtypes. However, because they usually rely on qualitative observations rather than predetermined quantitative thresholds, these diagnoses might be subjective. Without clear diagnostic thresholds, for instance, statements such as "low-to-moderate oedema could indicate tumor characteristics" are still ambiguous. As a result, tumor detection accuracy is still a major challenge, with existing techniques providing only mediocre reliability.

AI has been a key component of neuro-oncology in recent years, with the potential to segment and categorize tumor subtypes in addition to detecting cancers in MR images. This study uses a DenseNet-based Convolutional Neural Network (CNN) model to improve brain tumor identification. The efficacy of pre-trained DenseNet and ResNet architectures in precisely detecting and describing brain cancers was assessed by comparing their performance under various settings.

Keywords: brain tumor, glioma, magnetic resonance imaging, convolution neural network, dense net, and resent.

INTRODUCTION

An unchecked proliferation of aberrant tissue that creates a fibrous network inside the brain is called a brain tumor. Magnetic resonance imaging (MRI) is widely used by radiologists to identify and monitor brain tumors. However, it can be time-consuming and error-prone to manually analyze the enormous amount of MRI pictures and find malignancies, which could affect prompt and precise patient care. The diagnosis is made more difficult by the fact that tumor cells and healthy tissue might look alike. As a result, the demand for an automated tumor detection system with high accuracy is rising. This study investigates the classification of brain MRIs as either tumor-affected or healthy using the deep learning algorithms.

This study uses a convolutional neural network (CNN) that has already been trained to 2D brain MRIs to propose a method for brain tumor detection. For tumor location and subtype identification following detection, this method may employ segmentation and classification models. To effectively train the model, we employ different MR images with varying form, tumor size, location and intensities. We compare the model with other designs that use residual connections in order to assess the model's performance in more detail.

Every layer in a dense block is connected to every other layer in a revolutionary connection pattern found in a new CNN architecture known as DenseNet [1, 2]. This architecture enhances feature reuse, reduces model size, and lessens the likelihood of overfitting by granting each layer access to the feature maps of all previous layers. Additionally, the loss function can implicitly provide deep supervision by supervising individual layers thanks to DenseNet's shortcut pathways. DenseNet is ideal for pixel-level predictions because of these characteristics. When used in CNN architectures, dense blocks enhance performance by preserving information flow as network depth rises. As the distance between input and output layers grows, DenseNet's connectedness reduces this problem, enabling effective information transfer, in contrast to typical CNNs.

Our method uses a large pre-processed dataset of T1-weighted contrast-enhanced MR images to train DenseNet models. In order to minimize overfitting, the model's architecture is improved by varying the number of classification layers, layer layout, hyperparameters, and dropout layers. Furthermore, data augmentation is used to expand the number of MRI slices, which improves the accuracy and resilience of the model even more.

RELATED WORK

Magnetic resonance imaging (MRI) is widely utilized in medical imaging because it produces high-resolution, radiation-free images. This enables non-invasive evaluation of brain disorders by radiologists [8], [9]. On the other hand, the computer-Aided Diagnosis (CAD) method was created to help identify brain malignancies early without requiring human assistance. CAD systems use MRI image analysis to produce diagnostic reports that provide radiologists with guidance [10].

The CAD process in medical imaging has been greatly enhanced by deep learning (DL) and machine learning (ML) applications [11–13], increasing the precision of brain tumor diagnosis. Machine learning techniques are based on feature extraction, selection, and classification. Many feature extraction techniques, including contour, texture-based, thresholding, and clustering, are used to segment tumors in the skull [14]. These techniques particularly extract important information from MRI images to improve accuracy [15]. However, important information may be lost during feature extraction [16].

By using the source images directly [17], DL approaches overcome this constraint and do away with the requirement for manually created features. Image features can be efficiently extracted by Convolutional Neural Networks (CNNs), a DL model with many convolution layers [18], [19]. Medical imaging frequently lacks huge datasets, despite CNNs' superior performance with them [20]. This problem is lessened by transfer learning, which helps achieve accuracy with little data by employing a model that has already trained on a dataset for classification [21], [22].

CNNs eliminate the need for human feature extraction techniques by offering a segmentation-free method. As a result, researchers have developed a number of CNN architectures, particularly for multiclass brain tumor identification. A 16-layer CNN model, for instance, was presented by [24] and evaluated on two publicly accessible datasets. A novel CNN-based method outperformed six machine learning models with a prediction accuracy of 97.9% after the tumor region was retrieved using the Fuzzy C-Means clustering algorithm [25].

CNNs have two main limitations even though they work effectively with large image datasets:

- Large image datasets are often required for training, which can be challenging in medical imaging.
- CNNs may struggle with image variations, such as rotation or tilt. This study addresses this by augmenting the dataset with new image variants.

Because only the fully linked layers need to be trained, this approach uses a pre-trained model with updated weights for classification, consuming less processing power. These benefits have led to the application of transfer learning models in the diagnosis of brain cancer. Talo et al., for example, used a pre-trained ResNet34 model to

differentiate between normal and pathological MRI brain pictures. They used significant data augmentation to obtain remarkable forecast accuracy [26].

METHODOLOGY

Fig. 1 describes the workflow utilized in this study to identify malignancy in MR images. To reduce noise and enhance picture quality, the MR images are first preprocessed. Through inverse filtering and noise smoothing, the Wiener filter is used to lower the mean square error. The contrast of the denoised photos is then improved via histogram equalization. A trained binary classifier is then used to detect tumors from these contrast-enhanced MRI images.

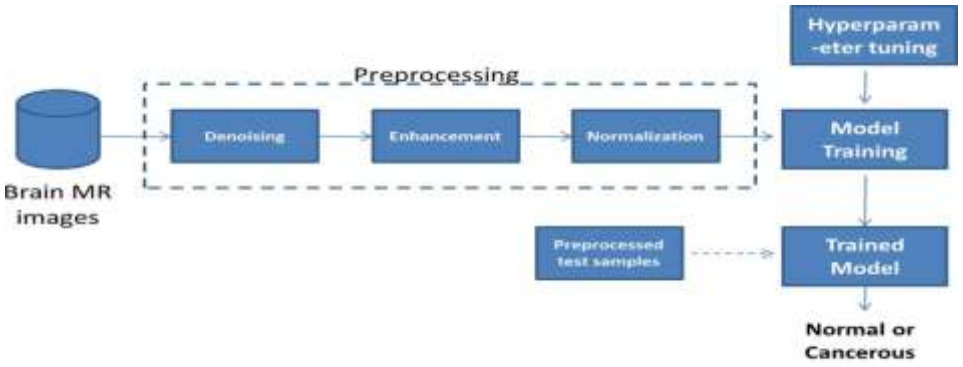

Fig. 1 Block Diagram of Brain Tumor Detection using Pre-trained Model

Three sources provided the MR image samples used in this investigation: the Br35H dataset, the SARTAJ dataset, and figshare. 9,523 MRI pictures of human brains divided into four classes meningioma, glioma, no tumor and pituitary are included in this integrated dataset. The Br35H dataset was especially used to source images for the "no tumor" class. Images classified as "no tumor" label as "0," while all other categories label as "1" to train the binary classifier. Training and testing were divided in an 80:20 ratio.

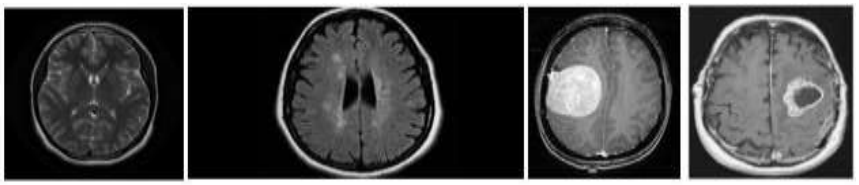

Fig. 2 **Sample Images a) & b) Normal c) & d) Tumorous images**

With the goal of minimizing the mean square error (MSE) between the output and the noise-free signal, the Wiener filter is an ideal linear filter that generates an output that closely resembles the original signal. Both noise and useful signal components are assumed to be present in the input, and they are both handled as generalized stationary processes with second-order statistical properties. The Wiener filter is a non-adaptive, frequency-domain implementation that treats noise and pictures as random processes. The filter's goal, which may be expressed as an optimization problem, is to minimize the MSE in order to estimate an ideal version of the original picture. Fig. 2 displayed the denoised image together with the corresponding raw image. This is how it is expressed mathematically:

$$\min e^2 = E\{(f - f')^2\} \qquad \text{Eq. 1}$$

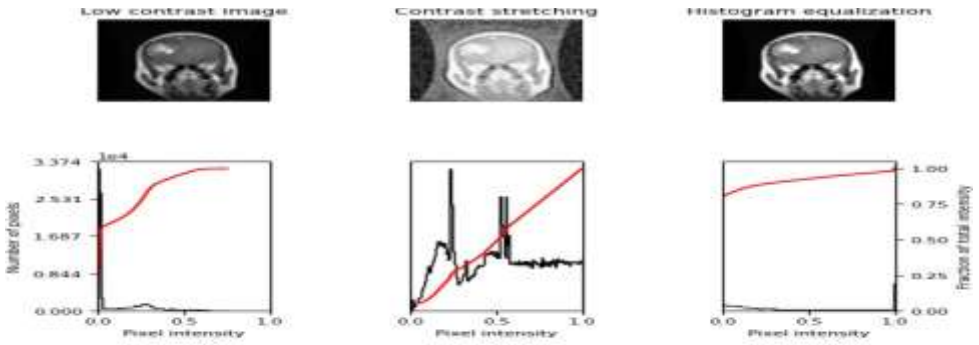

Fig. 3 Contrast enhancement using Histogram Equalization

the essential preprocessing technique for enhancing CAD in MRI is contrast enhancement. The Improving the original image's quality is the main goal of image enhancement, especially when it comes to emphasizing particular significant components. Histogram equalization, a method for enhancing low contrast photos, balances pixel distribution and increases the dynamic range of pixel values to produce a high contrast image [7]. This method is based on the fundamental idea of histogram equalization, which is the image's gray-level values' probability distribution [8]. The discrete function that represents the pixels of an image I ranges from 0 to L-1. The value of L for an 8-bit picture is 256.

The probability of appearance of gray scale r_k is

$$Pr(r_k) = \frac{n_k}{n} \; k = 0,1,2 \ldots \ldots, L-1 \qquad \text{Eq. 2}$$

where r_k represents the k^{th} gray level, n_k represents the count of pixels with r_k as gray level, and n is total number of pixels in the image.

The objective of the histogram equalization is to obtain a uniform distribution of the gray levels in the image. Ps(s) is a pdf of the image after equalization has been done. An equalized histogram, or Ps(s), has a constant distribution across all conceivable values. The following transfer function changes Pr(r) into Ps(s).

$$s = T(r) = (L-1)\int_0^r Pr(w)\,dw \qquad \text{Eq. 3}$$

By differentiating Eq. 3 with respect to r

$$\begin{aligned} \frac{ds}{dr} &= \frac{d}{dr}T(r) \\ &= \frac{d}{dr}(L-1)\int_0^r Pr(w)dw \\ &= (L-1)Pr(r) \end{aligned} \qquad \text{Eq. 4}$$

Relation between the probability distribution of raw and contrast enhanced image can be expressed as;

$$\begin{aligned} Ps(s) &= Pr(r)\left|\frac{ds}{dr}\right| \\ &= Pr(r)\left|\frac{1}{(L-1)Pr(r)}\right| \\ &= \frac{1}{(L-1)}; 0 \le L-1 \end{aligned} \qquad \text{Eq. 5}$$

By differentiating Eq. 3 with respect to r

Consequently, Ps(s) is a normalized distribution, and the histogram can be equalized using the transfer function provided in Eq. 3. Fig. 3 displays the outcome of histogram equalization.

The DenseNet Architecture

Every layer in the DenseNet architecture is intimately connected to every other layer, facilitating an effective information flow across the network. The vanishing gradient problem that frequently arises in models with many layers is lessened by this design. DenseNets, which use fewer parameters than traditional CNNs, concentrate on feature reuse rather than creating deep or wide topologies to increase representational capacity. DenseNets use fewer parameters than conventional CNNs because of their architecture, which eliminates the need for redundant feature maps. DenseNets address issue by adding only a few additional feature maps per layer, but ResNet versions have demonstrated that many layers contribute minimally. Because each layer receives direct gradient information from the input and the loss function, DenseNets can handle very deep networks efficiently thanks to this minimalistic architecture, improved information flow, and gradient access.

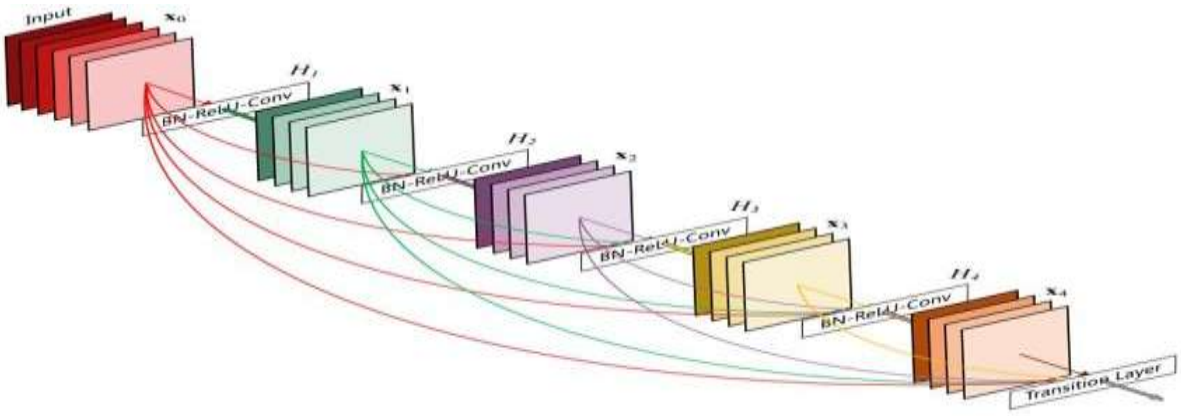

Fig. 4 Schematic view of connection pattern in DenseNet [5]

Traditional feed-forward neural networks use a series of composite processes, usually including an activation function, batch normalization, and either a convolution or pooling operation, before sending the output of each layer sequentially to the following layer. The following is a mathematical expression for this composite operation

$$x_l = H_l(x_{l-1}) \quad \text{Eq. 6}$$

Expanding this behavior by including the skip connection, ResNets reformulated this operation as follows;

$$x_l = H_l(x_{l-1}) + x_{l-1} \quad \text{Eq. 7}$$

DenseNets concatenate rather than sum the layer's output feature maps and incoming feature maps. As a result, the equation changes once again to;

$$x_l = H_l(x_0, x_1, \ldots\ldots, x_{l-1}) \quad \text{Eq. 8}$$

DenseNets are divided into DenseBlocks, where the number of filters varies from block to block but the dimensions of the feature maps remains constant inside each block. Transition Layers are the layers in between them that handle the downsampling by performing batch normalization, 1x1 convolution, and 2x2 pooling layers. Every layer of the feature maps' concatenation results in an increase in the channel dimension. If the H_l layer consistently generates k feature maps, it is possible to generalize this to the $l - th$ layer as follows;

$$k_l = k_0 + k * (l - 1) \quad \text{Eq. 9}$$

Each layer has access to both its prior feature maps and the collective knowledge. Each layer then contributes additional data to this body of knowledge in the form of concrete k feature maps of information. Fig.5 provides a very basic representation of the architecture of the DenseNet-121, which was utilized in this work.

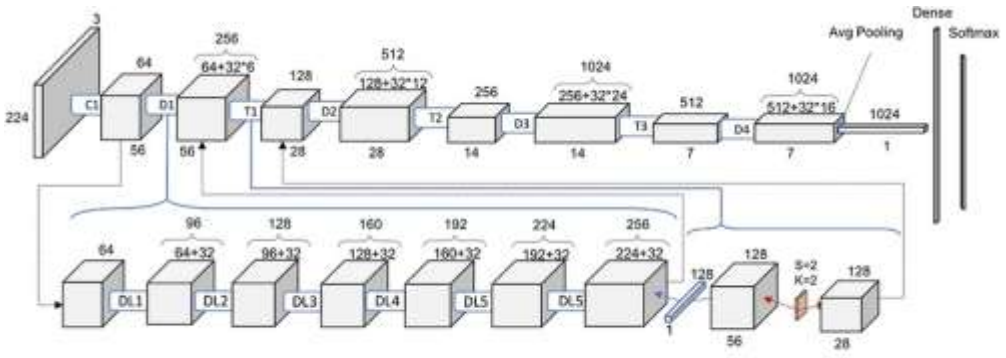

Fig. 5 Schematic view of Dense and Transition Blocks in a DenseNet-121 architecture [6]

Transition Block operates as a 1x1 convolution with 128 filters. The volume and quantity of feature maps are split in half after a 2x2 pooling with a stride of 2.

EXPERIMENT AND OUTCOME

To increase the batch size and learning rate in this investigation, a random search was employed. Potential values were found as contenders after the search; assessing these candidates aided in identifying the optimal range. The ideal batch size and learning rate were selected for the model's training based on the outcomes of the random search. The datasets were trained using the DenseNet model with bottleneck layers, compression, and a growth rate of 12. Batch sizes ranged from 16 to 128 and the learning rate varied from 0.001 to 0.1. The model was trained for 50 epochs with weight decay set to 0.0001 and momentum set to 0.9.

Transfer learning is an effective deep learning method that accelerates learning and improves model accuracy by using model parameters that have previously been trained on a larger dataset. In this scenario, only training the fully linked layers and leaving the CNN layers frozen allowed for faster training and higher performance customized to brain MRI images. Pre-trained weights were adjusted to account for the special features of this brain MRI dataset. Convolutional layers, batch normalization (BN), and a rectified linear unit (ReLU) activation layer make up a dense block in the DenseNet architecture. The last dense block is followed by a global average pooling layer that is linked to a Softmax classifier. In a DenseNet with L layers, each pair of layers has a direct connection with every other pair, for a total of $L(L+1)/2$ connections.

The Batch normalization was used to normalize the activations or the inputs of a previous layer. Dense blocks with similar sizes but different filter configurations make up DenseNet. Batch normalization is done by a Transition Layer that downsamples. Average pooling down-samples are carried out by figuring out the average value of each feature map segment. Weights were changed throughout training by the Adamax optimizer, and the loss function was Cross Entropy. Adamax, an extension of the Adam optimization technique, produces efficient optimization by modifying gradient descent to the infinite norm.

DISCUSSIONS

The algorithm successfully distinguished between photographs with brain tumors and those that were healthy after it had been trained to classify images it had never seen before. The trained model produced dependable classification accuracy for the test photos by reducing validation loss. As seen in Fig. 6, the addition of a denoising step in pre-processing employing a Wiener filter enhanced model performance. The model's accuracy for the brain tumor and healthy classes was evaluated using recall, F1-score, accuracy, and precision metrics. Furthermore, the model's performance was contrasted with that of other CNN designs and optimization techniques, including ResNet and Inception.

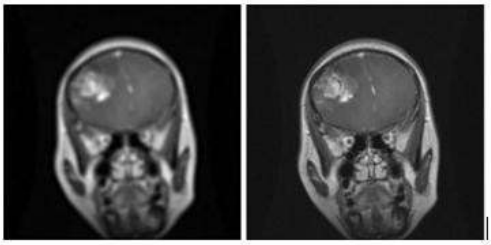

Fig. 6 Result after Denoising using weiner filter a. Raw image and b) Denoised image

The model's training accuracy is dependent on the sample photos used. Model performance over epochs is depicted in Fig. 7, which consistently shows an increase in accuracy with increasing epochs. DenseNet outperformed ResNet-50 and Inception V3, which obtained 86.3% and 76.2% accuracy, respectively, to earn the greatest training accuracy of 91.94%. Despite the inclusion of dropout, batch normalization, and regularization approaches, the notable discrepancy between Inception V3's validation and training accuracies raises the possibility of overfitting.

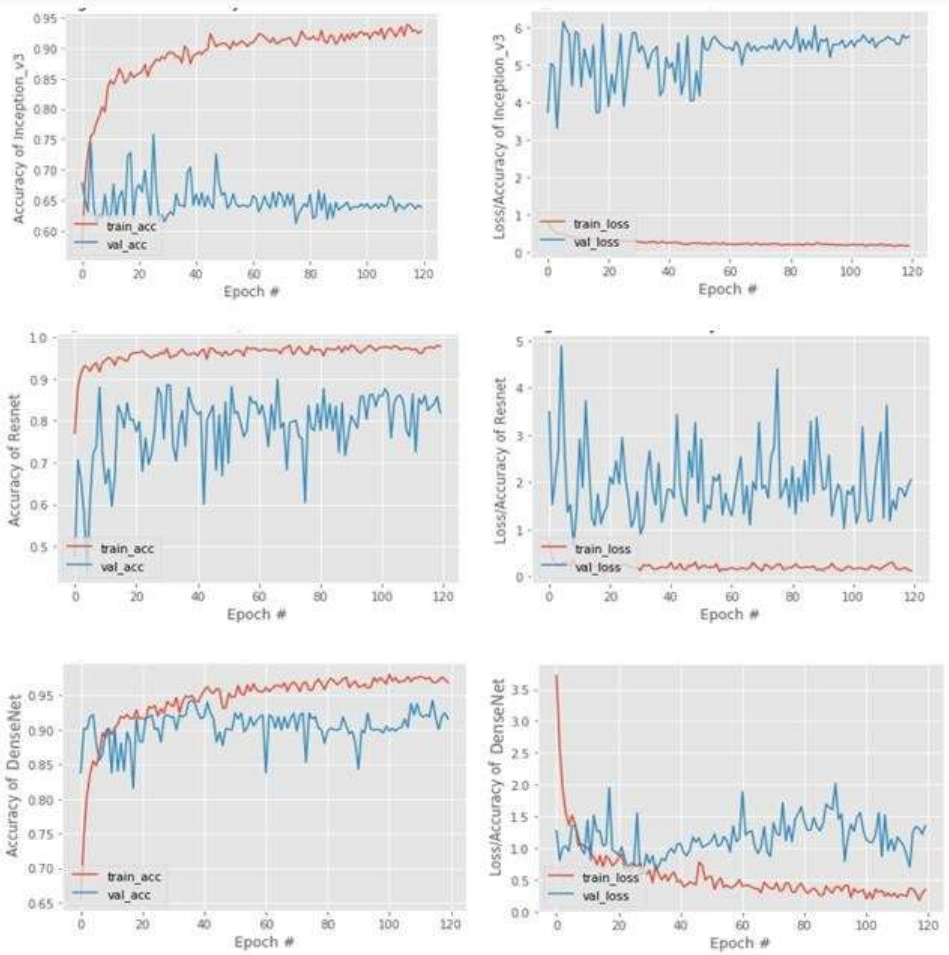

Fig. 7 Training and Validation performance of CNN Architectures

In this case, training loss demonstrates which attributes to include and how well the model is learning with each iteration. to lower mistakes and enhance the model's capacity to differentiate between brain tumors and typical cases in later rounds. When differentiating brain tumor patients from healthy cases, a The DenseNet model is highly accurate and generates less errors when the loss value is smaller.

Table. 1 Performance Comparison of DenseNet model

Model	Accuracy	Precision	Recall	F1 Score	AUC RoC
DenseNet	0.90	0.84	0.97	0.90	0.91
Inception V3	0.76	0.74	0.82	0.78	0.71
ResNet	0.86	0.81	0.91	0.85	0.81

The identity shortcut that stabilizes training limits the representational capacity of ResNet, but multi-layer feature concatenation gives DenseNet a larger capacity. The results in Table 1 show that our suggested model outperforms ResNet by a wide margin. Several optimization procedures are used to further evaluate the DenseNet design's robustness, and the outcomes are listed in Table 2.

Table. 2 Performance Comparison of DenseNet model with various optimization algorithm

Model	Accuracy	Precision	Recall	F1 Score	AUC RoC
ADAMAX	0.90	0.84	0.96	0.88	0.90
ADAM	0.88	0.85	0.92	0.86	0.88
SGD	0.85	0.84	0.81	0.83	0.86

AdaMax's primary benefit over SGD is its significantly lower sensitivity to hyper-parameter selection. AdaMax employs the ADAM estimate method's second momentum component. This provides a weight optimization problem solution that is more reliable. To address the gradient descent issue, Stochastic Gradient Decent (SGD) was created, which adjusts parameters with a single record. However, because each record must propagate both forward and backward, SGD takes a long time to converge. Because to his weight degradation, Adam is not always able to make the best decisions. Consequently, The model trained with the ADAMAX optimizer produced superior results in terms of accuracy, precision, and other metrics, as was evident from the results.

FINAL RESULT

The DenseNet architecture and CNN suggested as useful methods for MRI-based brain tumor diagnosis. A systematic review of papers pertaining to deep learning-based diagnostic techniques is becoming more and more necessary as the prevalence of brain illnesses and related research increases. This study aims to assist researchers and educators by offering a quantitative analysis of relevant literature. A comparative analysis was also conducted to automatically select the optimal optimizer, and the findings indicated that Adamax outperformed Adam and SGD. To choose the best learning rates and batch sizes for our trials, we employed a random search strategy. The findings showed that the DenseNet model can be trained well with 64 batch size and with 0.01 optimal learning rate. These values demonstrated their efficacy in training with an average accuracy of almost 90%.

REFERENCES

[1] Zhang, C., et al. "ResNet or DenseNet? Introducing Dense Shortcuts to ResNet." *IEEE Winter Conference on Applications of Computer Vision (WACV)*, Waikoloa, HI, USA, 2021, pp. 3549-3558.

[2] Zhu, Y., & Newsam, S. "DenseNet for Dense Flow." *IEEE International Conference on Image Processing (ICIP)*, IEEE, 2017.

[3] Nazir, M., Shakil, S., & Khurshid, K. "Role of Deep Learning in Brain Tumor Detection and Classification (2015 to 2020): A Review." *Computerized Medical Imaging and Graphics*, vol. 91, 2021, p. 101940.

[4] Amin, J., et al. "Brain Tumor Detection and Classification Using Machine Learning: A Comprehensive Survey." *Complex & Intelligent Systems*, 2021, pp. 1-23.
[5] Huang, G., Liu, Z., & Van der Maaten, L. "Densely Connected Convolutional Networks," 2018.
[6] Towards Data Science. "Understanding and Visualizing DenseNets." [Online]. Available: https://towardsdatascience.com/understanding-and-visualizing-densenets-7f688092391a.
[7] Kaur, H., & Sohi, N. "A Study for Applications of Histogram in Image Enhancement." *The International Journal of Engineering and Science (IJES)*, vol. 6, no. 6, 2017, pp. 59-63.
[8] Banu, R.A.K., & Ram, A.R. "Contrast Enhancement of MRI Images: A Review." *International Journal of Emerging Technology and Advanced Engineering (IJETAE)*, vol. 5, no. 6, 2015.
[9] Gudigar, A., et al. "Application of Multiresolution Analysis for Automated Detection of Brain Abnormality Using MR Images: A Comparative Study." *Future Generation Computer Systems*, vol. 90, 2019, pp. 359-67.
[10] Chen, Y., et al. "A Feature-Free 30-Disease Pathological Brain Detection System by Linear Regression Classifier." *CNS & Neurol Disorders-Drug Targets*, vol. 16, no. 1, 2017, pp. 5-10.
[11] Chen, Y., et al. "Sensorineural Hearing Loss Detection via Discrete Wavelet Transform and Principal Component Analysis." *Multimedia Tools and Applications*, vol. 77, no. 3, 2018, pp. 3775-3793.
[12] Wang, S.-H., et al. "Multiple Sclerosis Detection Based on Biorthogonal Wavelet Transform, RBF Kernel Principal Component Analysis, and Logistic Regression." *IEEE Access*, vol. 4, 2016, pp. 7567-7576.
[13] Islam, S., et al. "SGBBA: An Efficient Method for Prediction System in Machine Learning Using Imbalance Dataset." *International Journal of Advanced Computer Science and Applications*, vol. 12, no. 3, 2021.
[14] Shah, F.M., et al. "Brain Tumor Segmentation Techniques on Medical Images—A Review."
[15] Komura, D., & Ishikawa, S. "Machine Learning Methods for Histopathological Image Analysis." *Computational and Structural Biotechnology Journal*, vol. 16, 2018, pp. 34-42.
[16] Leng, W.Y., & Shamsuddin, S.M. "Writer Identification for Chinese Handwriting." *International Journal of Advanced Soft Computing Applications*, vol. 2, no. 2, 2010, pp. 142-173.
[17] Arif, M., et al. "Brain Tumor Detection and Classification by MRI Using Biologically Inspired Orthogonal Wavelet Transform and Deep Learning Techniques." *Journal of Healthcare Engineering*, 2022.
[18] Alsaif, H., et al. "A Novel Data Augmentation-Based Brain Tumor Detection Using Convolutional Neural Network." *Applied Sciences*, vol. 12, no. 8, 2022, p. 3773.
[19] Almadhoun, H.R., & Abu-Naser, S.S. "Detection of Brain Tumor Using Deep Learning." *International Journal of Academic Engineering Research*, vol. 6, no. 3, 2022.
[20] Sa, R., et al. "Intervertebral Disc Detection in X-Ray Images Using Faster R-CNN." *Annual International Conference of the IEEE Engineering in Medicine and Biology Society (EMBC)*, IEEE, 2017, pp. 564–567.
[21] Anjum, S., et al. "Detecting Brain Tumors Using Deep Learning Convolutional Neural Network with Transfer Learning Approach." *International Journal of Imaging Systems and Technology*, vol. 32, no. 1, 2022, pp. 307-323.
[22] Alanazi, M.F., et al. "Brain Tumor/Mass Classification Framework Using MRI-Based Isolated and Developed Transfer Deep-Learning Model." *Sensors*, vol. 22, no. 1, 2022, p. 372.
[23] Shin, H.-C., et al. "Deep Convolutional Neural Networks for Computer-Aided Detection: CNN Architectures, Dataset Characteristics, and Transfer Learning." *IEEE Transactions on Medical Imaging*, vol. 35, no. 5, 2016, pp. 1285-1293.
[24] Sultan, H.H., et al. "Multi-Classification of Brain Tumor Images Using Deep Neural Network." *IEEE Access*, vol. 7, 2019, pp. 69215-69225.
[25] Hossain, T., et al. "Brain Tumor Detection Using Convolutional Neural Network." *IEEE Conference*, 2019.
[26] Talo, M., et al. "Application of Deep Transfer Learning for Automated Brain Abnormality Classification Using MR Images." *Cognitive Systems Research*, vol. 54, 2019, pp. 176-188.